A Theoretical Study of Sensitizer Candidates for Dye-Sensitized Solar Cells: Peripheral Substituted Di-Zn-Pyrazinoporphyrazine-Phthalocyanine Complexes.

ARTICLE *in* THE JOURNAL OF PHYSICAL CHEMISTRY A · DECEMBER 2012

Impact Factor: 2.69 · DOI: 10.1021/jp3067316 · Source: PubMed

4 AUTHORS:

Ximena Zarate
Universidad Autónoma De Chile
32 PUBLICATIONS **90** CITATIONS
SEE PROFILE

Eduardo Schott
Pontifical Catholic University of Chile
50 PUBLICATIONS **295** CITATIONS
SEE PROFILE

Tatiana Gomez
Universidad Autónoma De Chile
10 PUBLICATIONS **83** CITATIONS
SEE PROFILE

Ramiro Arratia-Perez
Universidad Andrés Bello
149 PUBLICATIONS **1,201** CITATIONS
SEE PROFILE

THE JOURNAL OF PHYSICAL CHEMISTRY A

Article

pubs.acs.org/JPCA

Theoretical Study of Sensitizer Candidates for Dye-Sensitized Solar Cells: Peripheral Substituted Dizinc Pyrazinoporphyrazine–Phthalocyanine Complexes

Ximena Zarate,* Eduardo Schott, Tatiana Gomez, and Ramiro Arratia-Pérez*

Departamento de Ciencias Químicas, Facultad de Ciencias Exactas, Universidad Andres Bello, Republica 275, Santiago, Chile

Supporting Information

ABSTRACT: We have carried out a theoretical study of the geometrical and electronic structures of a family of planar dimers constituted by zinc(II) pyrazinoporphyrazine and zinc(II) phthalocyanine with peripheral electron-donating and electron-withdrawing substituents R [where R = —OH (**1**), —$C(CH_3)_3$ (**2**), —CH_3 (**3**), —C_6H_5 (**4**), —H (**5**), —CO_2H (**7**), —NO_2 (**7**), and —PO_3H_2 (**8**)]. The complexes are connected by varying the bridge (B) ligand, where, in **1**–**9**, B is —CH═ and, in **10**–**12**, B is —N═, —O—, and —S—, respectively. The —CO_2H group was included in complexes identified as **9**–**12**. This was done because of the known properties of this group in acting as an anchor to adsorb a dye onto a semiconductor oxide. The aim of this work was to provide a useful theoretical basis for the design and screening of new potential dye candidates to be used in these devices, based on the properties of the dyes suitable for their good performance in solar cells, such as frontier molecular orbital spatial distributions; charge-separated states in the electronic transitions in the visible region of the spectrum; and importantly, the energy diagram of the frontier MOs of these dyes and the conduction band (CB) of the semiconductor, where the LUMO energy levels that are above of the CB suggest which dyes are capable of electron injection into TiO_2. In this sense, it is expected that complexes **1**–**5** and **9**–**12** should be very promising dyes to act as sensitizers. Finally, a linear correlation was found between the HOMO and LUMO energies of all of the systems and the Hammett constants, where these molecular orbitals become more stable when R is more electron-withdrawing.

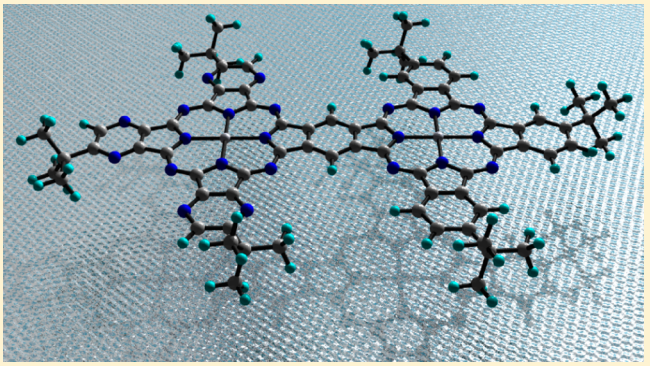

INTRODUCTION

Porphyrins and phthalocyanines are targets of interest in areas such as photocatalysis, catalysis, and energy conversion devices, among others.[1−4] For these reasons, considerable efforts have been made to synthesize new structures that might show improved molecular properties. In addition, theoretical studies have been performed to better understand the optical, electronic, and magnetic properties of metal-free complexes, coordinated to metals (such as Zn, Ni, Co, Ti, Ru, and Al) and also dimers of these macrocycles linked by bridges.[1−6] Moreover, attention has been focused on the formation of ordered thin-film assemblies, such as those constituted by dimers or heterodimers of porphyrins (P), porphyrazines (Pz), and phthalocyanines (Ph) connected by different bridges/linker groups including benzene ring, naphthalene ring, or mutual chelation of a metallic ion.[4−7] Some bridges help to keep rigid coplanar configurations of the systems, which generally exhibit spectroscopic and electrochemical properties that occasionally are significantly different from those of their monomer parents. Among their applications, these macrocycles are considered to be excellent sensitizers in the design of dye-sensitized solar cells (DSSCs), because of its good performance in light-harvesting devices.[8−11] DSSCs are mainly composed of nanocrystalline films of semiconductor oxides with wide band gaps (i.e., TiO_2 and ZnO) and a layer of dye attached to this semiconductor surface. Electron injection into the conduction band (CB) of the semiconductor occurs after photoexcitation of the dyes, during which the dye is oxidized. This oxidized dye is regenerated by the iodide/triiodide redox couple. Finally, the iodide is regenerated by the reduction of triiodide at the counter electrode, where the electrons that come from the load of the circuit are supplied to complete the cycle.[12−17]

In a DSSC device, the dyes are chemically bonded to the semiconductor through anchoring groups such as carboxylic or phosphonic acid (CO_2H or PO_3H_2), among others.[12] Moreover, there are other important features for efficient electron injection from the dye to the semiconductor, that is, the charge separation states that are generated in the dye and can be analyzed through the compositions of the frontier molecular orbitals (MOs). Here, the HOMO (highest occupied molecular orbital) is localized in the donor subunit of the molecule and the LUMO (lowest unoccupied molecular orbital) is localized

Received: July 6, 2012
Revised: December 18, 2012
Published: December 30, 2012

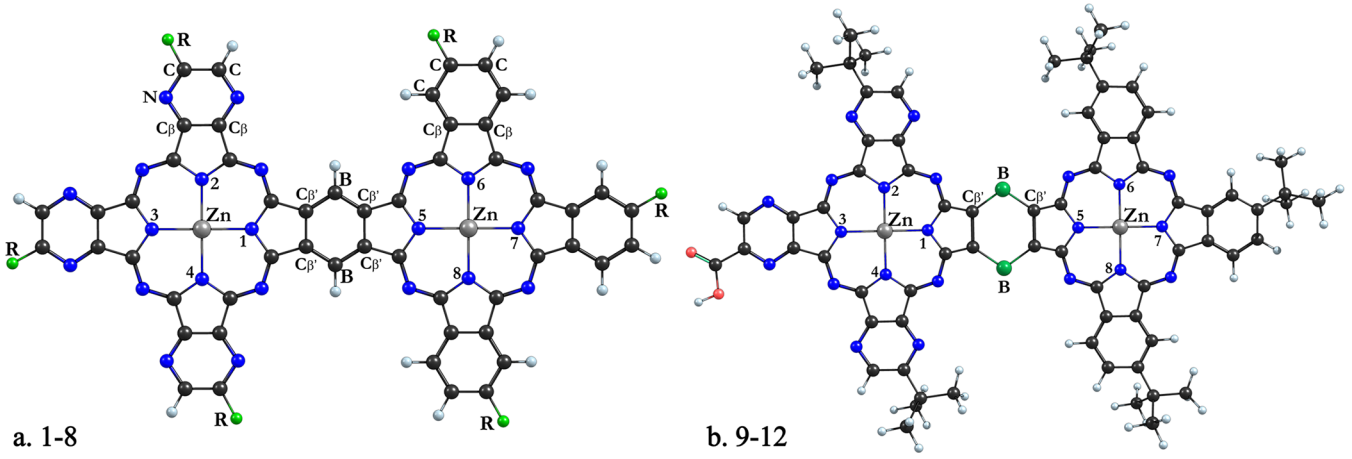

Figure 1. General molecular structure of the dizinc pyrazinoporphyrazine–phthalocyanine complexes (a) R = ——OH (**1**), —$C(CH_3)_3$ (**2**), —CH_3 (**3**), —C_6H_5 (**4**), —H (**5**), —CO_2H (**6**), —NO_2 (**7**), and —PO_3H_2 (**8**) and (b) with different bridge atoms B = —CH═ (**9**), —N═ (**10**), —O— (**11**), and —S— (**12**). The labels employed for the description of geometrical parameters are also shown.

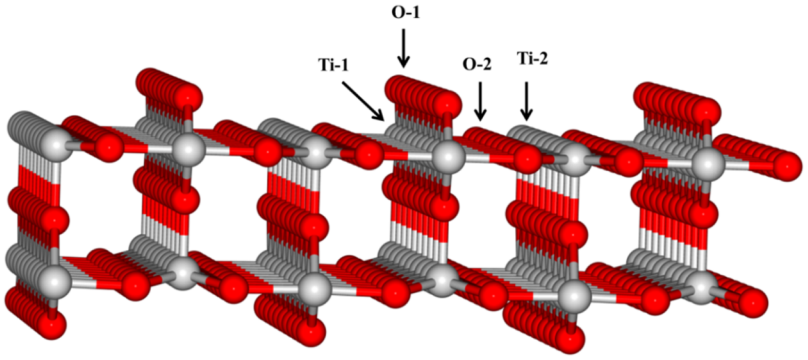

Figure 2. Ball-and-stick representation of the TiO_2(110) rutile surface.

over the subunit that contain the anchoring group.[3,11,13] Furthermore, the LUMO energy of the dye should lie above of the energy of the bottom of the CB of TiO_2.[4,14−16] Donor−acceptor π-conjugated compounds have been shown to exhibit photoinduced intramolecular charged transfer-properties that can facilitate rapid electron injection from the dye molecule into the CB of the semiconductor.

On the other hand, research groups have studied dimer macrocycles as sensitizers, because it has been demonstrated that they cover most of the superficial area, and thus, they have been used in the design of thinner dye-sensitized films. Koehorst et al.[8] reported the first enhanced spectral response of porphyrin-dimer-sensitized TiO_2 films. Also, these cells are an attractive technology in applications such as rooftop or window solar collectors, although this research area still has a way to go before it can be used in large-scale devices. Thus, it is valuable to propose sensitizer candidates for DSSCs to optimize and handle their properties.

In this work, a theoretical study of a family of dimers dizinc pyrazinoporphyrazine−phthalocyanine complexes with different peripheral substituents (R) and different atoms in the bridge (B) is presented. The aim of this work was to study the effect of the substituents and of the bridge on properties such as electronic structure, orbital composition and optical properties, among others. The results are focused on the requirements of the dyes to act as good sensitizers in DSSCs.

The systems with different peripheral substituents R are enumerated as follows: —OH (**1**), —$C(CH_3)_3$ (**2**),[18] —CH_3 (**3**), —C_6H_5 (**4**), —H (**5**), —CO_2H (**6**), —NO_2 (**7**), and —PO_3H_2 (**8**). In addition, we studied the complexes with R = —$C(CH_3)_3$, changing B and including over the Pz ring the —CO_2H anchoring group. These latter systems were enumerated as follows with B equal to —CH═ (**9**), —N═ (**10**), —O— (**11**), and —S— (**12**) (see Figure 1).

To study the substituent effects, it was taken into account the HOMO and LUMO energy dependence of all the systems versus the Hammett constants (σ). The σ values were defined by Hammett[19,20] from the ionization constants of benzoic acids as follows

$$\sigma_X = \log(K_X) - \log(K_H) \quad (1)$$

where K_H is the ionization constant for benzoic acid in water at 25 °C and K_X is the corresponding constant for a substituted benzoic acid.

The constant measures the capacity to perturb the electronic environment. One of the postulates is that the electronic effects of substituents over the molecule consist of an inductive component and a resonance component. Earlier studies showed a good correlation between the Hammett constants and properties such as the half-wave potential for the first oxidation and the first reduction potential of β-substituted copper(II) tetraphenylporphyrins[21] and the isotropic shift of the low-spin pyrrole resonance in β-substituted iron(III) tetraphenylporphyrin complexes.[22]

As this study is directed toward proposing a series of molecules that might show good properties for behaving as

dx.doi.org/10.1021/jp3067316 | J. Phys. Chem. A 2013, 117, 430−438

Table 1. Average Values of Selected Bond Distances (Å) and Angles (deg) of the Molecular Structures of Complexes 1−12[a]

parameter[b]	1	2	3	4	5	6	7	8	9	10	11	12
Zn—N[a]	2.015	2.015	2.016	2.017	2.016	2.017	2.017	2.017	2.015	2.018	2.011	2.010
Zn—N[b]	2.012	2.010	2.012	2.010	2.012	2.011	2.012	2.010	2.010	2.012	2.010	2.006
C_β—C_β[a]	1.411	1.410	1.412	1.420	1.416	1.416	1.416	1.417	1.408	1.407	1.408	1.409
C_β—C_β[b]	1.413	1.410	1.412	1.413	1.415	1.415	1.415	1.415	1.410	1.410	1.409	1.411
C_β'—C_β'	1.425	1.425	1.425	1.425	1.424	1.424	1.423	1.424	1.425	1.429	1.372	1.380
C_β'—B	1.392	1.393	1.393	1.393	1.393	1.392	1.393	1.393	1.393	1.336	1.376	1.757
C—R	1.359	1.532	1.505	1.495	1.092	1.501	1.510	1.834	1.531	1.531	1.532	1.531
C_β—N—C[a]	113.5	114.7	114.2	113.9	113.1	113.4	112.9	113.5	114.7	114.6	114.7	114.7
C_β—C—C[b]	117.3	119.4	118.9	118.5	117.8	117.7	116.4	117.7	119.2	119.1	119.3	119.3
C_β'–B—C_β'	115.8	115.8	115.8	115.7	115.8	115.6	115.6	115.6	115.8	111.4	108.4	97.9

[a]In complexes **1**−**9**, B is —CH═; in complexes, **10**−**12** B is —N═, —O—, and —S—, respectively. [b]Superscript a indicates Pz, b indicates Ph.

good sensitizers in DSSCs, the TiO_2(110) rutile surface was modeled with the band structure approach using periodic boundary conditions (see Figure 2). Thus, it was possible to construct an energy diagram with the energies of the frontier molecular orbitals of the dyes and to compare these energies with the CB of the modeled TiO_2(110) surface (see Figure 6, below). The dyes bonded to the semiconductor will be the subject of future studies.

COMPUTATIONAL METHODS

Molecular Systems. *Quantum Chemical Calculations.* The calculations were performed at the density functional theory (DFT) level, as implemented in the Amsterdam Density Functional package (ADF 2010).[23] Relativistic corrections were included through the zeroth-order regular approximation (ZORA) Hamiltonian.[24,25] Slater-type orbital (STO) basis sets with triple-ζ accuracy plus polarization function (TZP) for all of the atoms were employed.[26,27] The molecular geometries of the ground states were fully optimized through the generalized gradient approximation (GGA) employing the BP86 functional.[28,29] Dimer **2** was previously characterized experimentally,[18] and it was used as the starting point in the geometry optimizations, changing the R substituents and the B atoms (Figure 1).

The excitation energies and oscillator strengths were estimated by time-dependent DFT (TD-DFT)[30,31] employing the van Leeuwen−Baerends (LB94) potential.[32] For the charge distribution calculations, three algorithms were employed: classical Mülliken, Hirshfeld, and Voronoi cell population analysis.[33,34]

Conceptual DFT. A branch of DFT has been developed since the late 1970s and early 1980s, called "Conceptual DFT" by R. G. Parr.[35] Based on the idea that the electron density is the fundamental quantity for describing atomic and molecular ground states, Parr and co-workers and, later, a large community of chemically orientated theoreticians initiated the formulation of a theory of chemical reactivity that has gained increasing attention in the literature. Several chemical concepts, for example, electronegativity and chemical hardness, received a firm theoretical foundation in the conceptual DFT context.[35,36]

In a well-known publication by Parr and co-workers,[35] conceptual DFT was presented in which the electronic chemical potential μ (eq 2) was identified as the partial derivative of the system's energy with respect to the number of electrons at a fixed external potential $v(r)$. From this point, using higher-order derivatives, quantities such as the chemical hardness η (eq 3), among others, were derived and used in chemical reactivity

$$\mu = \left(\frac{\partial E}{\partial N}\right)_{v(r)} \tag{2}$$

$$\eta = \frac{1}{2}\left(\frac{\partial^2 E}{\partial N^2}\right)_{v(r)} = \frac{1}{2}\left(\frac{\partial \mu}{\partial N}\right)_{v(r)} \tag{3}$$

As noted above, the indexes arise from the energy E, and the derivatives of $E[N,v(r)]$ respect to N and $v(r)$ produce global quantities that allow the concepts of reactivity and selectivity to be quantified. In numerical applications, μ and η are calculated through the following approximate versions based on the finite-difference approximation and Koopmans' theorem[37]

$$\mu \approx -\frac{1}{2}(I + A) \approx \frac{1}{2}(\varepsilon_L + \varepsilon_H) \tag{4}$$

$$\eta \approx \frac{1}{2}(I - A) = \frac{1}{2}(\varepsilon_L - \varepsilon_H) \tag{5}$$

where I and A are the ionization energy and electron affinity, respectively, and ε_H and ε_L are the energies of the HOMO and LUMO, respectively.

The electrophilicity index ω is a measure of the propensity of a system to acquire electronic charge from the surroundings.[38] It is defined as

$$\omega = \frac{\mu^2}{2\eta} \tag{6}$$

μ is a global property that characterizes the escaping tendency of an electron from a system in its ground state; it is related to the negative of the absolute electronegativity. The concept of η was introduced in relation to the study of generalized Lewis acid−base reactions. The criterion used was that Lewis acids would form more stable compounds with donor systems with high electronegativity, whereas other class of Lewis acids would preferably interact with donor systems with low electronegativity. This is essentially related to polarizability, leading to the classification of "hard" (low polarizability) and "soft" (high polarizability).

On the other hand, the capability to accept one electron from a donor is measured by electron affinity, so ω is thought of as a sort of "electrophilicity power".

Surface Model. Periodic calculations were performed using the Vienna ab Initio Simulation Package, VASP 4.6,[39−41] using the GGA with the exchange and correlation energy proposed by Perdew and Wang (PW91).[28] A plane-wave basis set was used to span the valence electronic states, and the core electrons were represented by the projected augmented wave

dx.doi.org/10.1021/jp3067316 | J. Phys. Chem. A 2013, 117, 430−438

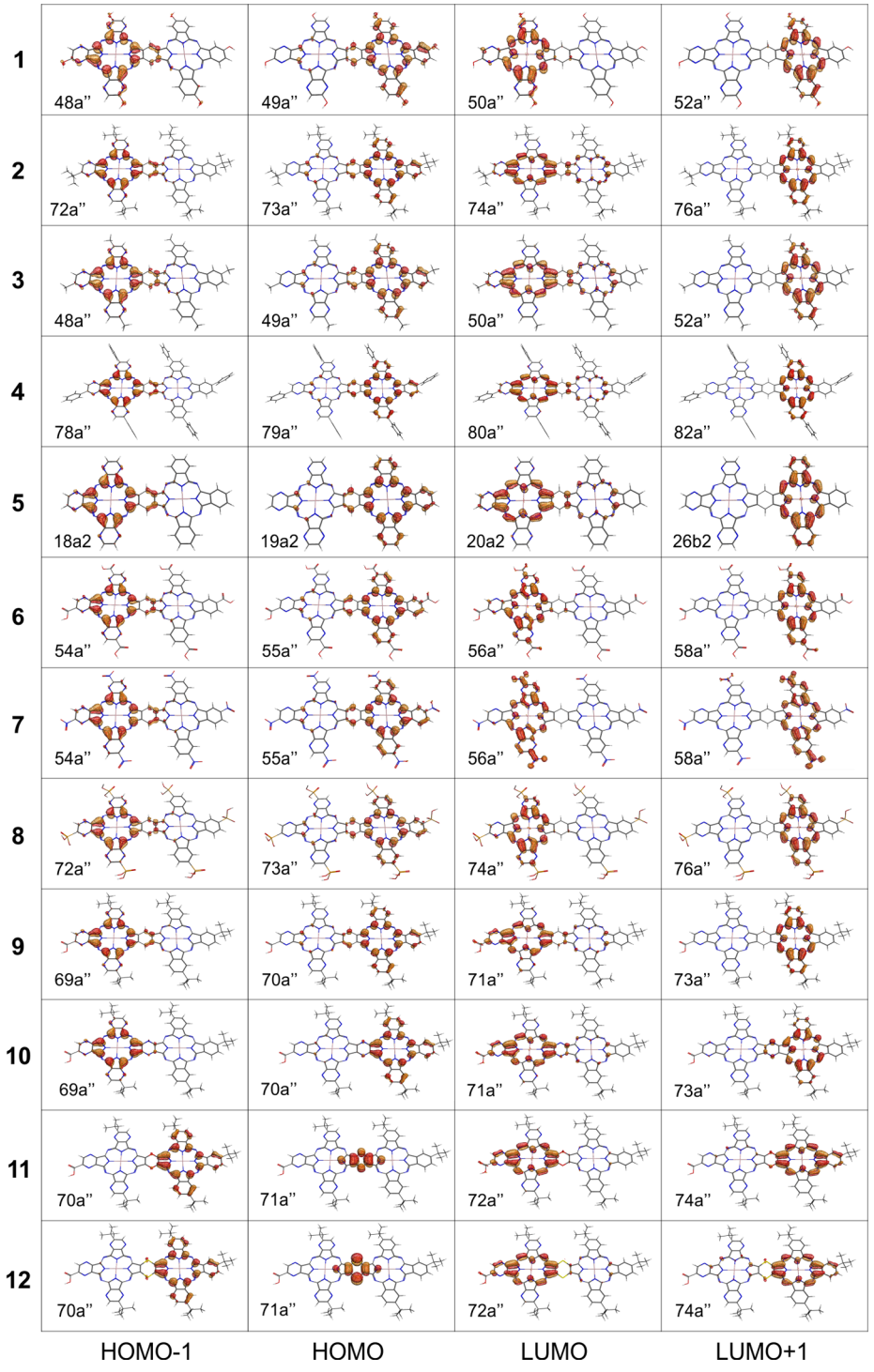

Figure 3. Calculated frontier MO isosurfaces of complexes **1**−**12**.

(PAW) method of Blöchl.[42] Two pseudopotentials were used to describe the titanium atoms. The first one describes 10 electrons ($3p^6 4s^2 3d^2$) and is referred to as PAW-Ti-sv in the pseudopotentials taken from the VASP library and PAW-Ti-10 here. The second one describes only four valence electrons ($3d^2 4s^2$) and is referred to as PAW-Ti-pv and labeled as PAW-Ti-4. For oxygen atoms, a PAW pseudopotential with six valence electrons ($2s^2 2p^4$) was used. A Monkhorst−Pack grid was used to select the special k points necessary to carry out numerical integrations in reciprocal space.

RESULTS AND DISCUSSION

Molecular Structure. The molecular structures of the dimeric dizinc pyrazinoporphyrazine−phthalocyanine complexes with peripheral substituents R were optimized. The substituent R groups are defined as electron-donating or electron-withdrawing depending on their σ values [electron-donating —OH (**1**), —$C(CH_3)_3$ (**2**), —CH_3 (**3**), —C_6H_5 (**4**); electron-withdrawing —CO_2H (**6**), —NO_2 (**7**), and —PO_3H_2 (**8**)].

dx.doi.org/10.1021/jp3067316 | J. Phys. Chem. A 2013, 117, 430−438

Calculated geometrical parameters are reported in Table 1. In general, the Zn—N distances in Pz are slightly longer than the Zn—N distances in Ph; this can be explained by the presence of the pyrazine, which is the only structural difference between the macrocycles. The C_{β}'—C_{β}' distances that are involved in the linkage of the macrocycles are slightly longer than the C_{β}—C_{β} distances. The main changes shown by the geometrical parameters are observed in the C—R distances, where the shortest is shown in **5** and the largest is presented in **8**. This increment in the bond distances is mainly due to steric effects generated by the R groups.

In all compounds, the angles formed by C—C—C in the Ph ring are larger (around 4°) than the C—N—C angles in the Pz ring. When B is —CH═, all of the C_{β}'–B—C_{β}' angles are around 118°. In contrast, for **9**–**12**, the C_{β}'–B—C_{β}' angles vary significantly (see Table 1).

On the other hand, the central metal Zn(II) lies over the plane formed by four central nitrogen atoms of each macrocycle. Thus, complexes **5** and **1** display C_{2v} symmetry, and the rest of the complexes were constrained to the C_s symmetry point group.

Electronic Structure. The isosurface plots of the frontier molecular orbitals (MOs), the highest occupied MOs (HOMO and HOMO − 1), and the lowest unoccupied MOs (LUMO and LUMO + 1) are presented in Figure 3.

In general, the frontier MOs show no contribution of the R substituents. The only exception is **7**, which shows a contribution from the R substituent because of its high electron-withdrawing nature. HOMO − 1 in complexes **1**–**10** is formed by p antibonding orbitals localized on the pyrrolic rings of Pz. By contrast, HOMO − 1 in complexes **11** and **12** is localized in the Ph macrocycle. The HOMO in complexes **1**–**10** is centered on the pyrrolic rings of the Ph macrocycle, and that in **11** and **12** is localized in the bridge region. In all complexes, the LUMO is localized in the Pz, and LUMO + 1 is localized over the Ph. The frontier MO composition indicates that, in molecules **1**–**10** that contain a donor moiety (HOMO), a bridge/linker group, and an acceptor moiety (LUMO), the electronic transitions with low energy might involve well-separated states. This is in agreement with calculations of coplanar dimers of zinc(II) tetraphenylporphyrins that have been demonstrated in solar cells showing efficient electronic injection.[3,10,43]

In conclusion, the effect of the different bridges is represented mainly in the localization of the HOMO in **11** (B = —O—) and **12** (B = —S—), where this orbital is composed of orbitals of the bridge fragment, unlike the frontier MOs in systems **1**–**9** (B = —CH═) and **10** (B = —N═) that do not show contribution of the B motifs. This points out that these last B motifs are able to generate a donor–bridge–acceptor system and display better performance in DSSCs than systems **11** and **12**. On the other hand, it is worth mentioning that it was also observed that the inclusion of the anchoring group (CO_2H) in systems **9**–**12** showed no dramatic change in the composition of the frontier MOs.

In the charge-transfer analysis of the Zn atoms, from **1** to **12** (Table S1, Supporting Information), the Mülliken, Hirshfeld, and Voronoi models showed charge donation from the ligands to the metallic centers in both macrocycles. The charge transfer to the metal obtained by Mülliken population analysis was greater than those obtained using the Hirshfeld and Voronoi models. These latter models have been reported as efficient methodologies for performing charge analysis.[33]

Zn(II) has the electronic configuration [Ar]$3d^{10}$. In the compounds investigated herein, where macrocycles coordinate the metal atoms, through calculated valence electronic configurations, we found charge donation to the s and p orbitals of the metals, which is expected because those macrocycles are predominantly π-donor ligand.

Time-Dependent DFT Analysis. The UV–vis absorption spectrum of a porphyrin is characterized by a weak Q band in the visible region and a B or Soret band at higher energy; in fact, the latter appears in the near-UV region together with the N band.[1] HOMO − 1, HOMO, LUMO, and LUMO + 1 are the MOs that are involved in the electronic transitions. They are commonly known as Gouterman orbitals.[44]

All complexes are peripherally substituted. Among the substituents we have —CH_3 and —$C(CH_3)_3$, which, through inductive effects, behave as electron donors. The —PO_3H_2, —NO_2, and —CO_2H groups, through both resonance and inductive effects behave as electron-withdrawing groups. By the resonance effect, —OH is electron-donating, and by the inductive effect, it behaves as electron-withdrawing. The phenyl group —C_6H_5 is electron-withdrawing by the resonance effect and electron-donating by the inductive effect.

The excitation energies, oscillator strengths, and compositions of the electronic transitions for complex **2** are reported in Table 2. The previously reported experimental values for absorption energies (in nanometers) are shown in parentheses next to the calculated data.[18] Complex **2** shows Q, B, and N bands in the experimental absorption spectra. The Q band splits into two intense bands and is red-shifted; this effect is greater for the dimers than for the monomers, which can be explained by the extension of the π-conjugated system.[1,5,18] All complexes show five bands in a large range of wavelengths (see Table S2, Supporting Information).

Table 2. Calculated Wavelengths (nm), Energies (eV), Oscillator Strengths *f*, Active MOs with Their Contributions (%), and Types of Electronic Transitions for the Vertical Excitations from TD-DFT for Complex 2

band	λ^a (nm)	*E* (eV)	*f*	active MO
Q	1050 (824)	1.15	0.493	(H–L) 73a″ → 75a″ (52.1), (H–L) 73a″ → 74a″ (36.9)
	744 (695)	1.67	0.666	[H–(L + 2)] 73a″ → 77a″ (49.5), [(H − 1)–L] 72a″ → 75a″ (18.1)
	722 (644 sh)	1.72	0.160	[H–(L + 1)] 73a″ → 76a″ (69.6), [(H − 1)–(L + 1)] 72a″ → 76a″ (23.5)
B	375 (356)	3.30	0.243	[(H − 9)–(L + 3)] 68a″ → 78a″ (79.5), [(H − 13)–L] 60a″ → 74a″ (5.2)
N	337 (294)	3.68	0.209	[(H − 11)–(L + 5)] 63a″ → 80a″ (32.9), [(H − 12)–(L + 5)] 62a″ → 80a″ (17.9), [(H − 10)–(L + 5)] 65a″ → 80a″ (10.1)

[a]Previously reported experimental data is in parentheses.

On the other hand, the accuracy of the calculations of electronic structures used to produce reliable calculated absorption spectra is highly dependent on the structural parameters used in the calculations. Our TD-DFT results show good agreement with experiment, which indicates a high accuracy in the electronic structure of the optimized systems, although the underestimation of the HOMO–LUMO gap using this methodology is evidenced in the energy under-

dx.doi.org/10.1021/jp3067316 | J. Phys. Chem. A 2013, 117, 430–438

estimation of the lowest-energy bands in the spectra, which are mainly composed of HOMO−LUMO transitions.

In the absorption spectra of complexes **1**−**8**, the intense B band and weak Q bands are mainly attributed to $\pi-\pi^*$ transitions. The Q band was assigned as a ligand-centered transition (LLCT, ligand-to-ligand charge transfer) where the transitions are HOMO−LUMO. The other bands in the visible region consist of a mixture of configurations with greater contributions from the HOMO−(LUMO + 1) and (HOMO − 1)−(LUMO + 1) transitions. In complexes **9**−**12**, the Q band is also LLCT, and the excitation is directed to the LUMO localized in the macrocycle that contains the anchoring group (—CO_2H). The B and N bands are composed of mixtures of configurations, which are of ML-LCT (metal−ligand-to-ligand charge transfer) type.

A plot of the Q bands of complexes **1**−**12** is shown in Figure 4. A red shift in the absorption spectra of **9**−**12** is observed as a result of a change in the bridge motif, keeping the electron-donating peripheral substituent [—$C(CH_3)_3$] on the macrocycles and adding an electron-withdrawing group that works as an anchor, which is advantageous for DSSCs applications. The Q band of **8** appears at the highest energy as compared to the other systems. All of the systems with electron-donating groups display a slight red shift with respect to system **2**.

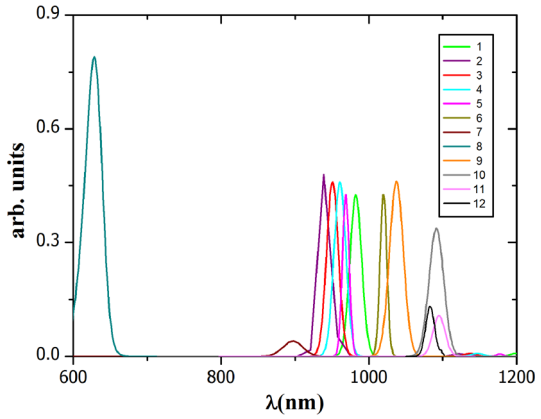

Figure 4. Plot of the Q bands for all of the studied complexes.

Reactivity Indexes. The derivative of E with respect to N and $v(r)$ produces global quantities that allow for the quantification of the concepts of reactivity and selectivity. These estimated reactivity indexes from the scalar relativistic calculations, electronic chemical potential (μ), chemical hardness (η), and electrophilicity (ω) are reported in Table 3. They arise from the energy $E[\rho(r)]$, which can be expressed in terms of the number of electrons N and the external potential $v(r)$. The electronic density $\rho(r)$ is the fundamental variable for obtaining the chemical observables; thus, their variations are related to the reactive behavior of a chemical system.

In general, the μ results indicate that systems **6**−**8** show less escaping tendency of the electrons from a system in equilibrium. Complexes **1**−**10** have similar η values, which can be interpreted as the resistance to the charge transfer of the system, whereas **11** and **12** show the smallest values, indicating that are the less hard complexes. The most electrophilic complexes are systems **6**−**8**, which have the most electron-withdrawing R groups, and **12** with B = —S— has the highest capability to accept one electron from a donor, showing the highest values of ω, which is thought of as a sort of electrophilicity power.[45]

Table 3. Frontier Molecular Orbital Energies (HOMO, LUMO, and HOMO−LUMO Gap) and Reactivity Indexes: electronic chemical potential μ, chemical hardness η and electrophilicity μ. (All values in eV)

complex	HOMO	LUMO	HOMO−LUMO gap	μ	η	μ
1	−5.04	−4.09	0.96	−4.57	0.48	21.78
2	−4.98	−3.95	1.02	−4.46	0.51	19.50
3	−5.04	−4.03	1.02	−4.53	0.51	20.19
4	−5.15	−4.13	1.02	−4.64	0.51	21.11
5	−5.23	−4.23	1.01	−4.73	0.50	22.21
6	−5.68	−4.76	0.92	−5.22	0.46	29.67
7	−5.70	−4.75	0.95	−5.22	0.48	28.66
8	−6.28	−5.32	0.95	−5.80	0.48	35.24
9	−5.08	−4.14	0.93	−4.61	0.47	22.75
10	−5.21	−4.27	0.94	−4.74	0.47	23.91
11	−5.07	−4.29	0.79	−4.68	0.39	27.78
12	−4.72	−4.27	0.45	−4.49	0.22	45.13

Hammett Correlations. The Hammett correlation was used to see the effect on the energy eigenvalues of the HOMOs and LUMOs of the R substituents in the molecules.[46,47]

A smooth and linear correlation of HOMO and LUMO energies with the sum of the Hammett parameters of the substituents on the ligand (σ) is presented in Figure 5. The effect on the frontier MOs when the substituent R is changed from electron-donating to electron-withdrawing is more stable HOMOs and LUMOs. These results are in agreement with previous theoretical studies of the effect of the substituent in zinc porphyrin monomers.[14,48] In porphyrinoid systems, the redox-potential shifts are linearly correlated with the Hammett parameters of the peripheral substituents. Electron-donating groups make the redox potential more negative, and electron-withdrawing groups make the redox potential more positive.[49] Therefore, systems with electron-donating substituents might transfer electrons easily, that is, the occupied orbitals display higher energies relative to macrocycles with electron-withdrawing groups.

These energy tendencies suggest that the observed energy changes in the frontier MOs due to β-substitution are correlated with the character of the R group, specifically with the Hammett parameters. The evaluated properties change almost linearly with the Hammett constants, and it is possible to predict the energy behavior of the frontier MOs in this kind of system depending on the character of the substituents, employing their Hammett constants.

TiO_2 Surface. The tetragonal unit cell of rutile TiO_2 contains two Ti and four O atoms, and it is characterized by the lattice parameters a and c (Table S3, Supporting Information). In the calculations of these parameters, the number of k points and the energy cutoff were checked for convergence with respect to the bulk relaxation, until total energies computed with increasing sets of k points differed by less than 0.01 eV. The optimal k-point mesh was 4 × 4 × 4 with a cutoff of 415 eV. The atomic relaxations for the bulk were performed at a constant volume to optimize atom positions in the lattice and to determinate equilibrium bulk parameters and reference energies; relaxations with unconstrained volume were performed. Once the lattice parameters were determined, a model for the TiO_2(110) surface was constructed using a slab

dx.doi.org/10.1021/jp3067316 | J. Phys. Chem. A 2013, 117, 430−438

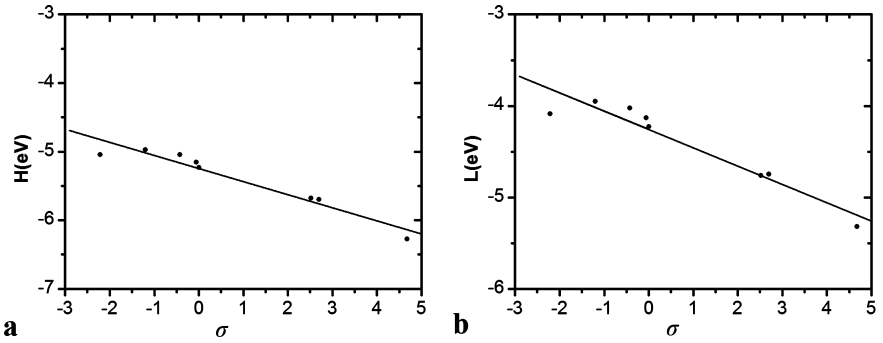

Figure 5. Hammett correlations of (a) HOMO (r = 0.933) and (b) LUMO (r = 0.919) energies versus sum of the Hammett parameters of the substituents on the ligand (σ).

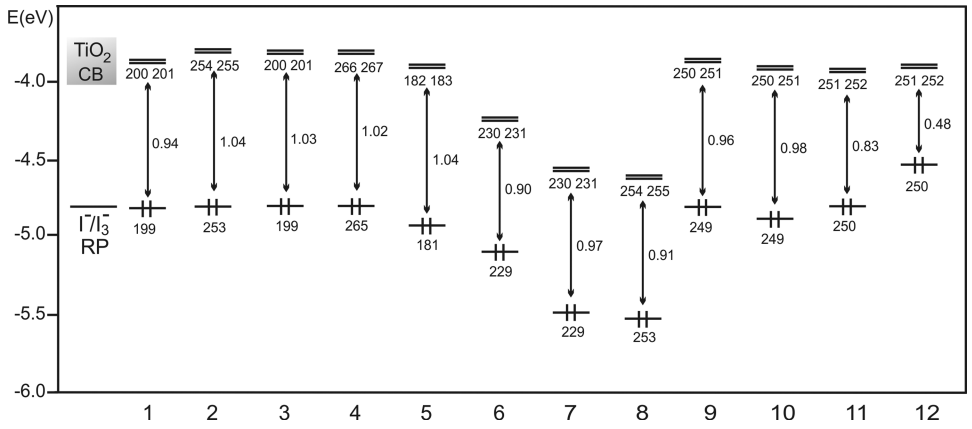

Figure 6. Energy level diagram of the HOMOs and LUMOs of complexes **1**−**12**.

model approach (see Figure 2). In this approach, the unit cell is repeated periodically in two dimensions, whereas it has a finite extent in the third. The vacuum width was increased until the energy variations were not significant. A 2 × 4 × 1 mesh of k points was used to sample the Brillouin zone of the 1 × 1 surface unit cell. Test calculations with a three times finer k sampling showed no changes in the slab geometry. All atoms were allowed to relax during the structure optimization.

We choose an 8 × 2 surface model of TiO_2(110); the grids of k points and the total numbers of atoms were centered at the Γ point (1 × 1 × 1) for (8 × 2) TiO_2(110) (360 atoms: 120 Ti, 240 O).

A band gap of 1.35 eV for the surface model of TiO_2(110) was calculated. The band gap value is far from that of bulk rutile TiO_2, with an experimental value of 3.05 eV,[50,51] which can be explained by the fact that self-consistent band structure calculations within DFT, using exchange and correlation GGA and LDA functionals, usually underestimate the energy gap (Table S4, Supporting Information).[52] It should be mentioned that the value of the band gap for the proposed surface model does not necessarily converge to the bulk value given the presence of more than one surface in the film.

The partial and total density of states (DOS) are plotted in the Supporting Information (Figure S1). The valence band (VB) is composed of σ-bonding states as a result of coupling between the 3d orbitals of the Ti and 2p orbitals of O. The VB has a bandwidth of 5.5 eV, which shows excellent agreement with the experimental value of 5.4 eV.[53] The top of the VB is mainly composed of the O 2p orbitals. On the other hand, the CB mainly consists of the 3d orbitals of Ti atoms. The states in the VB and CB have contributions from O 2p and Ti 3d orbitals; this indicates that both bands are involved in Ti—O σ-bond formation given by the hybridization between these states.

A diagram with the calculated energy value of the bottom of the TiO_2 CB (in gray) and the HOMO and LUMO energies for all of the systems calculated using a plane-wave basis set with the same theoretical level of the surface and the redox potential of the couple I^-/I_3^- is presented in Figure 6.[7,54,55] It is worth mentioning that it is possible to obtain a better description of the band gap, considering more explicit atoms in the construction of the surface or incorporation of the Hubbard (U) parameter.[56]

Based on the energetic requirement, which is that two different materials must have energy levels suitable for an electron transfer, it is seen in the energy level diagram (Figure 6) that the LUMOs energies of **1**−**5** and **9**−**12** reside above and close to the calculated CB, which indicates that these systems can show coupling with the semiconductor. Furthermore, all complexes show the HOMO level near the redox potential of the I^-/I_3^-, which is convenient for the regeneration of the dye.

CONCLUSIONS

The study of a family of dizinc porphyrazine−phthalocyanine complexes has been performed using relativistic scalar ZORA Hamiltonian, where their molecular and electronic structures were analyzed.

The calculations provided a useful theoretical basis for the design and the study of candidate analogues of commonly used dyes, based on molecular energy level diagrams, calculated absorption profiles, spatial distributions of orbitals, and

dx.doi.org/10.1021/jp3067316 | J. Phys. Chem. A 2013, 117, 430−438

reactivity indexes. We conclude that complexes **1**−**5** with electron-donating peripheral substituents, and **9** with R = —$C(CH_3)_3$ including the anchoring group —CO_2H as well as **10**−**12** (B = —N═, —O—, and —S—, respectively) are promising light-harvesting and sensitizing compounds for DSSC devices. The factors that were considered in the design of such molecules include electronic transitions (HOMO−LUMO) covering a long visible range of the spectra. Also, it is interesting to mention that most of the calculated transitions are composed of charge-separated states and hence donor−bridge−acceptor systems. Complexes **11** and **12** do not show this feature, which could affect the efficiency of the photoinjection process. All of these complexes show favorable LUMO energies leading to electron injection; these are lying just above the semiconductor CB. On the other hand, these complexes have shown high chemical potential (μ) and low electronegativity (ω) with respect to the systems with electron-withdrawing R substituents. The exception for this last statement is system **12**.

—CO_2H, which is used to adsorb the dyes to the semiconductor surface, could be added to the molecules without dramatic changes in the different properties that the sensitizers need to display in a DSSC.

The calculated geometrical parameters show that there is no major change in the macrocycles spite of the differences in the character of the peripheral substituents. In contrast, the HOMO isosurface is partially displaced to the substituent when it becomes more electron-withdrawing.

Substituents with different electron-donating or electron-withdrawing natures can be used to systematically tune the MO energy levels of porphyrins. This was observed through the linear correlation of the HOMO and LUMO energies with the Hammett constants.

The TiO_2 rutile surface was simulated, and the band gap energy and bandwidth were calculated. The calculated bandwidth was in very good agreement with the previously reported experimental value. These results provide a detailed description of the density of states (total and partial) that showed the composition of the valence and conduction bands. The CB of the TiO_2 surface was useful for building the energy level diagram.

■ ASSOCIATED CONTENT

Ⓢ Supporting Information

Charge-transfer analysis, simulated UV−vis spectra, bulk parameters and density of states of the TiO_2 surface. This material is available free of charge via the Internet at http://pubs.acs.org.

■ AUTHOR INFORMATION

Corresponding Author

*Phone: 56-2-6618232. E-mail: rarratia@unab.cl (R.A.-P.), jazminac@gmail.com (X.Z.).

Notes

The authors declare no competing financial interest.

■ ACKNOWLEDGMENTS

This work was funded by Project P07-006-F de la Iniciativa Científica Milenio del Ministerio de Economía, Fomento y Turismo, CONICYT, for doctoral fellowships awarded to X.Z. and E.S (Fondecyt 1110758 UNAB 17-11/R). X.Z. thanks Jorge Luis Zárate Bonilla.

■ REFERENCES

(1) Kobayashi, N. *Coord. Chem. Rev.* **2002**, *227*, 129−152.
(2) Mozer, A. J.; Griffith, M. J.; Tsekouras, G.; Wagner, P.; Wallace, G. G.; Mori, S.; Sunahara, K.; Miyashita, M.; Earles, J. C.; Gordon, K. C.; Du, L.; Katoh, R.; Furube, A.; Officer, D. L. *J. Am. Chem. Soc.* **2009**, *131*, 15621−15623.
(3) Walter, M. G.; Rudine, A. B.; Wamser, C. C. *J. Porphyrins Phthalocyanines* **2010**, *14*, 759−792.
(4) Zarate, X.; Schott, E.; Arratia-Pérez, R. *Int. J. Quantum Chem.* **2011**, *111*, 4186−4196.
(5) Baumann, T. F.; Barrett, A. G. M.; Hoffman, B. M. *Inorg. Chem* **1997**, *36*, 5661−5665.
(6) Cheng, K.; Thai, N. A.; Teague, L. C.; Grohmann, K.; Drain, C. M. *Chem. Commun* **2005**, *37*, 4678−4680.
(7) Imahori, H.; Umeyama, T.; Ito, S. *Acc. Chem. Res.* **2009**, *42*, 1809−1818.
(8) Koehorst, R. B. M.; Boschloo, G. K.; Savenije, T. J.; Goossens, A.; Schaafsma, T. J. *J. Phys. Chem. B* **2000**, *104*, 2371−2377.
(9) Lin, C. Y.; Wang, Y. C.; Hsu, S. J.; Lo, C. F.; Diau, E. W. G. *J. Phys. Chem. C* **2010**, *114*, 687−693.
(10) Sunahara, K.; Furube, A.; Katoh, R.; Mori, S.; Griffith, M. J.; Wallace, G. G.; Wagner, P.; Officer, D. L.; Mozer, A. J. *J. Phys. Chem. C* **2011**, *115*, 22084−22088.
(11) Campbell, W. M.; Jolley, K. W.; Wagner, P.; Wagner, K.; Walsh, P. J.; Gordon, K. C.; Schmidt-Mende, L.; Nazeeruddin, M. K.; Wang, Q.; Grätzel, M.; Officer, D. L. *J. Phys. Chem. C* **2007**, *111*, 11760−11762.
(12) Duncan, W. R.; Prezhdo, O. V. *Annu. Rev. Phys. Chem.* **2007**, *58*, 143−84.
(13) Wang, Q.; Campbell, W. M.; Bonfantani, E. E.; Jolley, K. W.; Officer, D. L.; Walsh, P. J.; Gordon, K.; Humphry-Baker, R.; Nazeeruddin, M. K.; Grätzel, M. *J. Phys. Chem. B* **2005**, *109*, 15397−15409.
(14) Ma, R.; Guo, P.; Cui, H.; Zhang, X.; Nazeeruddin, M. K.; Grätzel, M. *J. Phys. Chem. A* **2009**, *113*, 10119−10124.
(15) De Angelis, F.; Fantacci, S.; Selloni, A. *Nanotechnology* **2008**, *19*, 424002−424008.
(16) Grätzel, M. *J. Photochem. Photobiol. C: Photochem. Rev.* **2003**, *4*, 145−153.
(17) O'Regan, B.; Grätzel, M. *Nature* **1991**, *353*, 737−740.
(18) Kobayashi, N.; Higashi, Y.; Osa, T. *J. Chem. Soc., Chem. Commun.* **1994**, 1785−1786.
(19) Hammett, L. P. *J. Am. Chem. Soc* **1937**, *59*, 96−103.
(20) Hansch, C.; Leo, A.; Taft., R. W. *Chem. Rev* **1991**, *97*, 165−195.
(21) Binstead, R. A.; Crossley, M. J.; Hush, N. S. *Inorg. Chem* **1991**, *30*, 1259−1264.
(22) Wojaczynski, J.; Latos-Grazynski, L.; Hrycyk, W.; Pacholska, E.; Rachlewicz, K.; Szterenberg, L. *Inorg. Chem* **1996**, *35*, 6861−6872.
(23) *Amsterdam Density Functional (ADF)*, release 2010; Vrije Universiteit: Amsterdam, The Netherlands, 2010.
(24) van Lenthe, E.; Baerends, E. J.; Snijders, J. G. *J. Chem. Phys.* **1994**, *101*, 9783−9792.
(25) Velde, G. T.; Bickelhaupt, F. M.; van Gisberger, S.; Fonseca-Guerra, C.; Baerends, E. J.; Snijders, J. G.; Ziegler, T. *J. Comput. Chem.* **2001**, *22*, 931−967.
(26) Snijder, J. G.; Vernooijs, P.; Baerends, E. J. *At. Data. Nucl. Data Tables* **1981**, *26*, 483−509.
(27) Vernooijs, P. Snijders, J. G. Baerends, E. J. *Slater Type Basis Functions for the Whole Periodic System*; Internal Report; Free University of Amsterdam, Amsterdam, The Netherlands, 1981.
(28) Perdew, J. P.; Chevary, J. A.; Vosko, S. H.; Jackson, K. A.; Pederson, M. R.; Singh, D. J.; Fiolhais, C. *Phys. Rev. B* **1992**, *46*, 6671−6687.
(29) Perdew, J. P.; Yue, W. *Phys. Rev. B* **1986**, *33*, 8800−8802.
(30) Casida, M. In *Recent Advances in Density Functional Methods*; Chong, D. P., Ed.; World Scientific: Singapore, 1995; Vol. *1*, pp 155−192.
(31) Gross, E. K. U.; Kohn, W. *Adv. Quantum Chem.* **1990**, *21*, 255−291.

(32) van Leeuwen, R.; Baerends, E. J. *Phys. Rev. A* **1994**, *49*, 2421−2431.
(33) Guerra, C. F.; Handgraaf, J. W.; Baerends, E. J.; Bickelhaup, F. M. *J. Comput. Chem.* **2004**, *25*, 189−210.
(34) Nalewajski, R. F. *Phys. Chem. Chem. Phys.* **2002**, *4*, 1710−1721.
(35) Parr, R. G.; Donnelly, R. A.; Levy, M.; Palke, W. E. *J. Chem. Phys.* **1978**, *68*, 3801−3807.
(36) Feng, X.; Yu, J. G.; Liu, R. Z.; Lei, M.; Fang, W. H.; De Proft, F.; Liu, S. *J. Phys. Chem. A* **2010**, *114*, 6342−6349.
(37) Parr, R. G.; Yang, W. *Density Functional Theory of Atoms and Molecules*; Oxford University Press: New York, 1989.
(38) Parr, R. G.; von Szentpaly, L.; Liu, S. *J. Am. Chem. Soc.* **1999**, *121*, 1922−1924.
(39) Blochl, P. E. *Phys. Rev. B* **1994**, *50*, 17953−17979.
(40) Kresse, G.; Hafner, J. *Phys. Rev. B.* **1993**, *47*, 558−561.
(41) Kresse, G.; Furthmüller, J. *Comput. Mater. Sci.* **1996**, *6*, 15−50.
(42) Kresse, G.; Furthmuller, J. *Phys. Rev. B* **1996**, *54*, 11169−11186.
(43) Liang, W.; Qi, D.; Zhang, Y.; Jiang, J. *Phys. Chem. Chem. Phys.* **2011**, *13*, 1639−1648.
(44) Gouterman, M. *J. Chem. Phys.* **1959**, *30*, 1139−1161.
(45) Chamorro, E.; Perez., P.; De Proft, F.; Geerlings, P. *J. Chem. Phys.* **2006**, *124*, 044105−044111.
(46) Wang, L.; Moss, R. A.; Thompson, J.; Krogh-Jespersen, K. *Org. Lett.* **2011**, *13*, 1198−1201.
(47) Rincón, L.; Almeida, R. *J. Phys. Chem. A* **2012**, *116*, 7523−7530.
(48) Ma, R.; Guo, P.; Yang, L.; Guo, L.; Zhang, X.; Nazeeruddin, M. K.; Grätzel, M. *J. Phys. Chem. A* **2010**, *114*, 1973−1979.
(49) Ochoa, G.; Geraldo, D.; Linares, C.; Nyokongd, T.; Bediouie, F.; Zagal, J. H. *ECS Trans.* **2009**, *19*, 97−112.
(50) Pascual, J.; Camassel, J.; Mathieu, H. *Phys. Rev. Lett.* **1977**, *39*, 1490−1493.
(51) Cronemeyer, D. C. *Phys. Rev. B* **1952**, *87*, 876−886.
(52) Dufek, P.; Blaha, P.; Schwarz, K. *Phys. Rev. B* **1994**, *50*, 7279−7283.
(53) Kowalczyk, S. P.; Mefeely, F. R.; Ley, L.; Gritsyna, V. T.; Schirley, A. *Solid. State. Commun* **1977**, *23*, 161−169.
(54) Hagfeldt, A.; Grätzel, M. *Chem. Rev.* **1995**, *95*, 49−68.
(55) Grätzel, M. *Nature* **2001**, *414*, 338−344.
(56) Arroyo-de Dompablo, M. E.; Morales-García, A.; Taravillo, M. *J. Chem. Phys.* **2011**, *135*, 054503−054503−9.